electronic reprint

Journal of
Applied Crystallography
ISSN 0021-8898
Editor: **Anke R. Kaysser-Pyzalla**

Crystal structures and thermal expansion of α-$MgSO_4$ and β-$MgSO_4$ from 4.2 to 300 K by neutron powder diffraction

A. D. Fortes, I. G. Wood, L. Vočadlo, H. E. A. Brand and K. S. Knight

J. Appl. Cryst. (2007). **40**, 761–770

Copyright © International Union of Crystallography

Author(s) of this paper may load this reprint on their own web site or institutional repository provided that this cover page is retained. Republication of this article or its storage in electronic databases other than as specified above is not permitted without prior permission in writing from the IUCr.

For further information see http://journals.iucr.org/services/authorrights.html

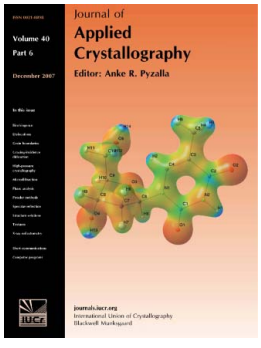

Many research topics in condensed matter research, materials science and the life sciences make use of crystallographic methods to study crystalline and non-crystalline matter with neutrons, X-rays and electrons. Articles published in the *Journal of Applied Crystallography* focus on these methods and their use in identifying structural and diffusion-controlled phase transformations, structure–property relationships, structural changes of defects, interfaces and surfaces, *etc.* Developments of instrumentation and crystallographic apparatus, theory and interpretation, numerical analysis and other related subjects are also covered. The journal is the primary place where crystallographic computer program information is published.

Crystallography Journals Online is available from **journals.iucr.org**

Journal of
Applied
Crystallography
ISSN 0021-8898

Received 7 September 2006
Accepted 19 June 2007

Crystal structures and thermal expansion of α-$MgSO_4$ and β-$MgSO_4$ from 4.2 to 300 K by neutron powder diffraction

A. D. Fortes,[a]* I. G. Wood,[a] L. Vočadlo,[a] H. E. A. Brand[a] and K. S. Knight[b,c]

[a]Department of Earth Science, University College London, Gower Street, London WC1E 6BT, UK, [b]ISIS Science Division, Rutherford Appleton Laboratory, Chilton, Didcot, Oxfordshire OX11 0QX, UK, and [c]The Natural History Museum, Cromwell Road, London SW7 5BD, UK. Correspondence e-mail: andrew.fortes@ucl.ac.uk

Detailed neutron powder diffraction measurements have been carried out on two polymorphs of anhydrous magnesium sulfate, α-$MgSO_4$ and β-$MgSO_4$. α-$MgSO_4$ is orthorhombic, space group *Cmcm* (Z = 4); at 4.2 K the unit-cell dimensions are a = 5.16863 (3), b = 7.86781 (5), c = 6.46674 (5) Å, V = 262.975 (2) Å^3 [ρ_{calc} = 3040.16 (2) kg m^{-3}], and at 300 K, a = 5.17471 (3), b = 7.87563 (5), c = 6.49517 (5) Å, V = 264.705 (2) Å^3 [ρ_{calc} = 3020.29 (2) kg m^{-3}]. The axial and volumetric thermal expansion coefficients are positive at all temperatures and exhibit no unusual behaviour. Structures were refined at 4.2 and 300 K to R_P < 3%; less precise structural parameters were determined during warming from 4.2 to 300 K. β-$MgSO_4$ has a more complex structure, crystallizing in space group *Pbnm* (Z = 4); the unit-cell dimensions at 4.2 K are a = 4.73431 (8), b = 8.58170 (12), c = 6.67266 (11) Å, V = 271.100 (5) Å^3 [ρ_{calc} = 2949.04 (5) kg m^{-3}], and at 300 K, a = 4.74598 (7), b = 8.58310 (10), c = 6.70933 (10) Å, V = 273.306 (4) Å^3 [ρ_{calc} = 2925.42 (4) kg m^{-3}]. The thermal expansivities of the a and c axes, and the volumetric thermal expansion coefficient, are positive at all temperatures and normally behaved. However, the thermal expansion of the b axis is both very small and negative below ~125 K. Structural and thermal motion parameters for β-$MgSO_4$ as a function of temperature are also reported.

© 2007 International Union of Crystallography
Printed in Singapore – all rights reserved

1. Introduction

There are three known polymorphs of anhydrous $MgSO_4$: two that co-exist below about 800 K (α and β) and one that is apparently stable above ~1273 K (γ). The phase that is grown from a solution of MgO in H_2SO_4 is called α-$MgSO_4$; its structure was solved initially by Rentzeperis & Soldatos (1958), being orthorhombic, with space group *Cmcm* (Z = 4) and unit-cell dimensions a = 5.182, b = 7.893, c = 6.506 Å ($CrVO_4$-type structure). Another phase, β-$MgSO_4$, may be formed either by dehydration of $MgSO_4$ hydrates or by heating α-$MgSO_4$ to 868 K (Yamaguchi & Kato, 1972); its structure, solved by Coing-Boyat (1962), is also orthorhombic, space group *Pbnm*, with unit-cell dimensions a = 4.742, b = 8.575, c = 6.699 Å ($ZnSO_4$-type structure). β-$MgSO_4$ can be quenched to room temperature, where it appears to persist (possibly metastably) indefinitely. Commercially available $MgSO_4$ is the β phase. Both α- and β-$MgSO_4$ are structurally very similar; each consists of edge-sharing MgO_6 octahedra arranged in infinite ribbons and cross-linked by sheets of pseudo-close-packed SO_4 tetrahedra, lying parallel to $(\bar{1}10)$ in the α phase but parallel to (010) in the β phase (Fig. 1). In α-$MgSO_4$, the octahedra between consecutive sheets are tilted in the same direction (Fig. 2*a*); however, each is offset slightly from the one below, the sequence being repeated every fourth layer (the packing is thus *ABCABC*). In β-$MgSO_4$, octahedra in consecutive layers are tilted in opposite directions but with a repeat sequence *ABABAB* (Fig. 2*b*).

A third phase, γ-$MgSO_4$, has been observed at temperatures above ~1273 K (Rowe *et al.*, 1967; Daimon & Kato, 1984). The structure of this phase is not known, an obvious possibility being that it might have the same structure as γ-$CoSO_4$ (the only other known sulfate with three polymorphs). However, Rowe *et al.* (1967) collected a diffraction pattern from the γ phase of $MgSO_4$, of which only five lines (out of 14) agree with the calculated pattern of γ-$CoSO_4$-type $MgSO_4$, which suggests that γ-$MgSO_4$ does not have the γ-$CoSO_4$ structure. In air, $MgSO_4$ decomposes to MgO + SO_3 at 1168 K, whereas in a sealed container the compound melts at ~1450 K.

Very little work exists on the bulk properties of $MgSO_4$ and the transition behaviour between α, β and γ phases. The thermal expansivity is unknown and no structural studies of the thermally induced phase transitions have been carried out. Livshits *et al.* (1963) compressed $MgSO_4$ (formed by dehydration of the heptahydrate) to ~3 GPa, but their low

electronic reprint

reported room P,T density is very close to that of $MgSO_4{\cdot}H_2O$ (kieserite), and so we must be cautious about accepting their results. Wang *et al.* (1999) compressed β-$MgSO_4$ to 7.7 GPa at 2073 K ($MgSO_4$ melts at 2223 K at 7.7 GPa); upon quenching, they observed an X-ray diffraction pattern from α-$MgSO_4$.

Magnesium sulfates may well be important planetary rock-forming materials in our solar system. $MgSO_4$ itself may be an important mineral in putative carbonatite lavas on Venus (Kargel *et al.*, 1994). In the outer solar system, $MgSO_4$ is the most important leachate from the chondritic materials which probably form the rocky cores of the large icy moons (Kargel, 1991). In the environment of an icy moon it is expected to be strongly hydrated, crystallizing salts such as $MgSO_4{\cdot}7H_2O$ (epsomite) and $MgSO_4{\cdot}11H_2O$ (meridianiite), which will compose the icy moons' mantles. Our goal to understand the structure and history of large icy moons requires knowledge of

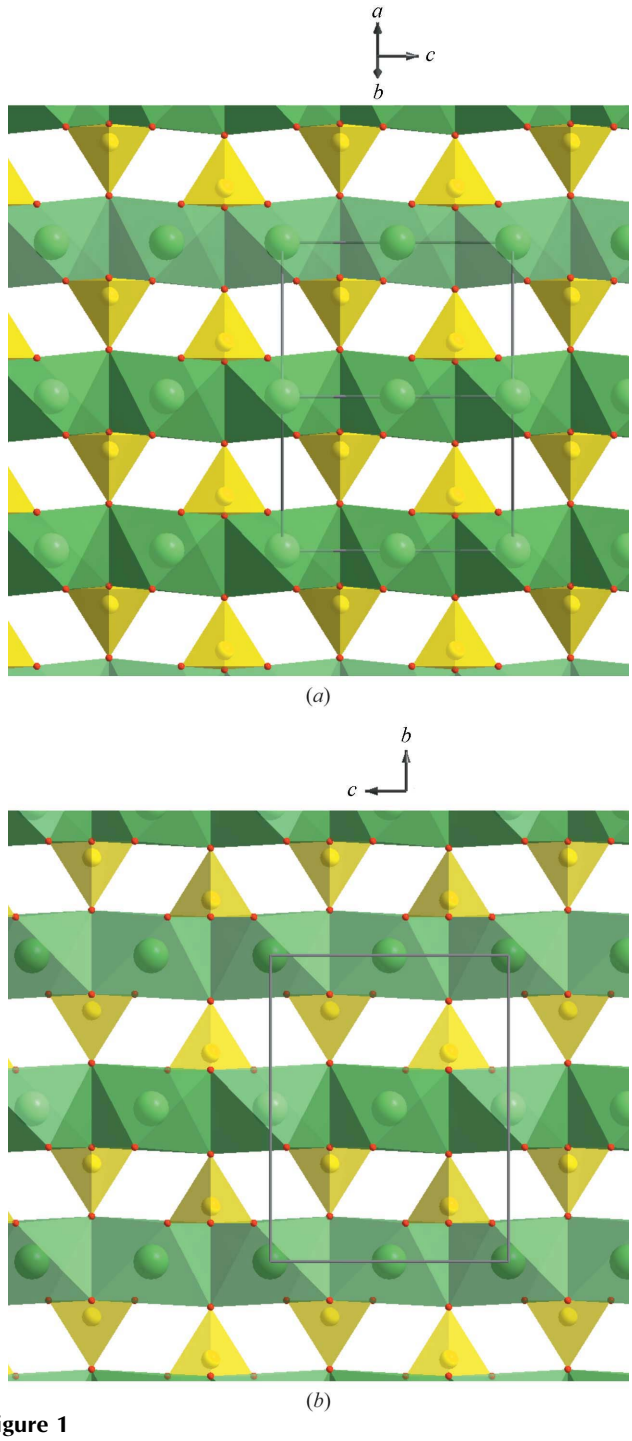

Figure 1
The structures of (*a*) α-$MgSO_4$ and (*b*) β-$MgSO_4$, in each case viewed perpendicular to the pseudo-close-packed layering in each phase, showing the chains of edge-sharing MgO_6 octahedra that extend along the *c* axes.

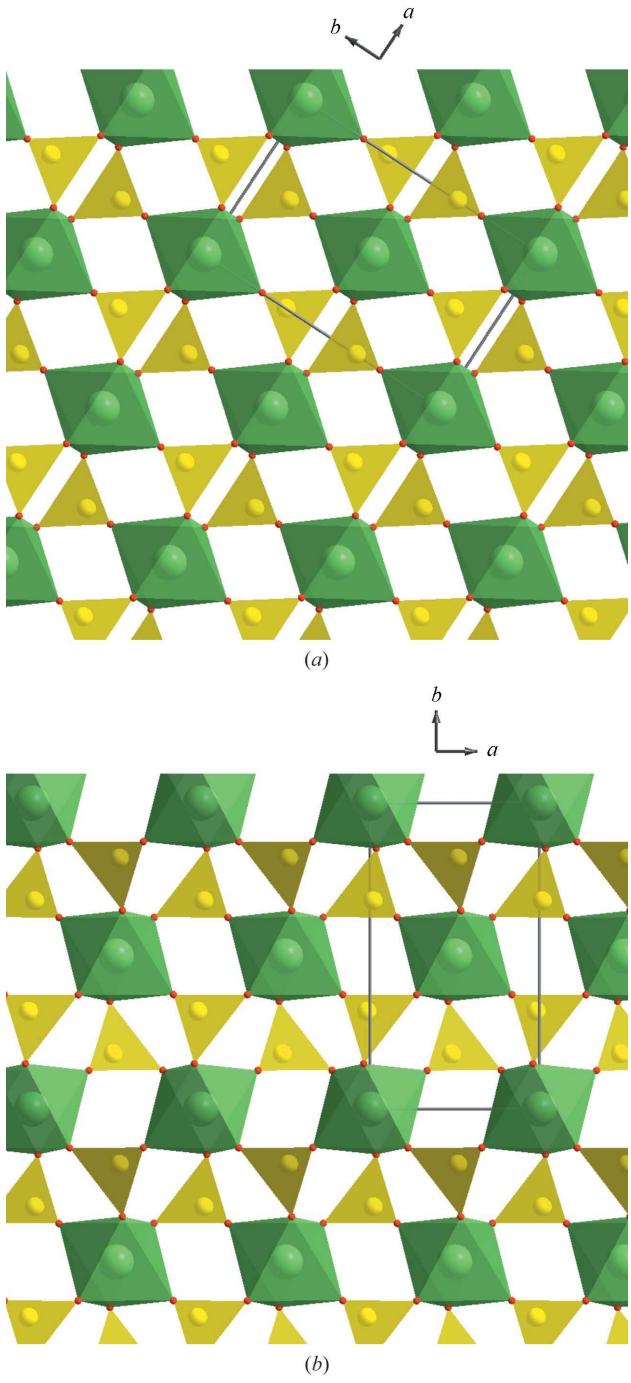

Figure 2
The structures of (*a*) α-$MgSO_4$ and (*b*) β-$MgSO_4$, in both cases viewed perpendicular to the pseudo-close-packed layering in each phase, showing the differences in packing of the layers.

electronic reprint

the physical properties of the constituent salts; we have therefore carried out a detailed neutron diffraction study of magnesium sulfate heptahydrate (Fortes *et al.*, 2006) and undecahydrate (Fortes *et al.*, 2004). This experimental work has been complemented by quantum mechanical computational simulation (Fortes *et al.*, 2006); however, *ab initio* calculations on crystals with such large unit cells (or low symmetry) are computationally very expensive indeed. We therefore wished to make detailed measurements of the physical properties of anhydrous $MgSO_4$, allowing us to fit Mg–O and S–O interatomic potentials without the added complication of bound water. Interatomic potential (IP) calculations will greatly extend our ability to understand the more complex $MgSO_4$ hydrates, which are so important in the outer solar system, at a greatly reduced computational cost.

To fit such potentials, we require accurate structural and thermoelastic data for all three $MgSO_4$ polymorphs. We are therefore carrying out *ab initio* calculations and also powder diffraction experiments as a function of temperature and pressure to measure these properties. As the first part of this study, we present the results of ambient-pressure neutron diffraction experiments on the α and β phases of $MgSO_4$ from 4.2 to 300 K. The paper commences by outlining the experimental method, followed by results and discussion.

2. Experimental method

2.1. Sample preparation

The β phase of $MgSO_4$ was supplied by Sigma (M7506, $\geq$ 99.5% anhydrous) and was dried at 673 K for 24 h. The specimen was examined by X-ray powder diffraction to confirm its structure and lack of water of hydration. α-$MgSO_4$ was prepared by mixing powdered MgO with H_2SO_4 in excess. The resulting dry powder was examined by X-ray powder diffraction and found to be a poorly crystalline hydrate of magnesium sulfate. The specimen was dried at 673 K for 24 h and thermogravimetric analysis revealed that three moles of water had been lost for every mole of $MgSO_4$. After drying, the X-ray diffraction pattern was that of α-$MgSO_4$.

2.2. Neutron powder diffraction

The neutron diffraction experiments were carried out at the STFC ISIS neutron spallation source, Rutherford Appleton Laboratory, Didcot, UK. All data were collected on the High Resolution Powder Diffractometer, HRPD (Ibberson *et al.*, 1992), which currently offers probably the best combination of flux and resolution available in the world. Low temperatures were achieved using a standard vanadium-tailed OC50 Orange cryostat, and the sample environment was an aluminium-framed slab-can with vanadium windows. The first sample can was packed with 4.4095 g of α-$MgSO_4$, the second with 5.006 g of β-$MgSO_4$; these were then screwed to a cryostat centre stick and loaded into the HRPD beamline before being equilibrated at a temperature of 4.2 K. Data were collected on the α and β phases at 4.2 K for 3 h (equivalent to 100 μA h of proton current) in the 30–130 ms time-of-flight window in both backscattering (2θ = 168.33°) and 90° detectors. After this, data were collected for shorter periods (10 μA h) at 10 K intervals during warming to 300 K (with three minutes of thermal equilibration at each interval). Finally, data were collected at 300 K for 3 h (100 μA h) for α-$MgSO_4$ and (owing to beamtime constraints) 2.5 h (80 μA h) for β-$MgSO_4$. The data were normalized to the incident monitor spectrum, corrected for detector efficiency using a vanadium standard and corrected for absorption using the measured packing density of the specimens.

2.3. Data analysis

All of the diffraction data were analysed using the *General Structure Analysis System* (*GSAS*; Larsen & Von Dreele, 1988). For the data sets recorded with long counting times at 4.2 K we allowed the unit cell, atomic coordinates and isotropic displacement parameters (U_{iso}) to refine, along with scale factors, background and peak profile coefficients. The background was fitted with a five-term shifted Chebyschev polynomial (*GSAS* background function 1). The peak profiles were modelled using the *GSAS* type 3 coefficients, varying σ_1 and γ_1 in backscattering and σ_1, σ_2 and γ_2 in the 90° banks. In addition, for the data collected in the 90° detectors, we also

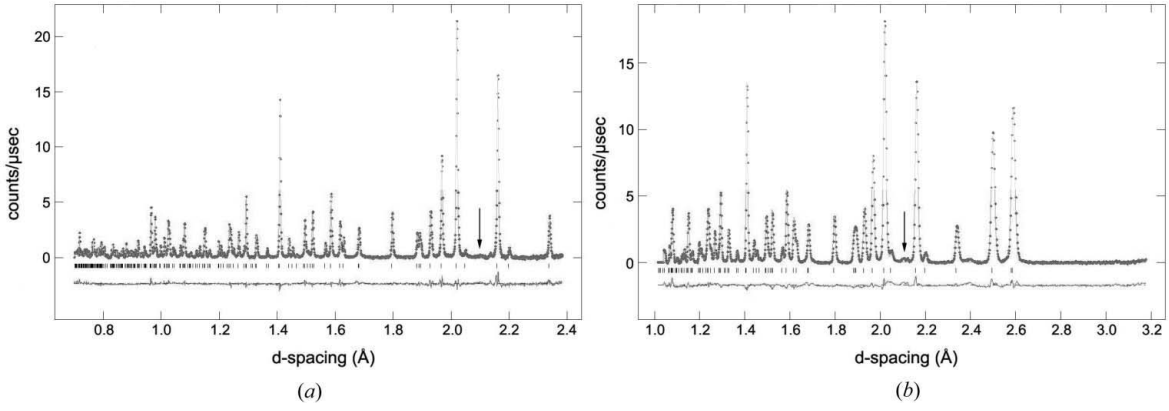

Figure 3
Powder diffraction data (points), Rietveld refinement (solid line fitted through the data), difference profile and tic marks (bottom) for α-$MgSO_4$ at 4.2 K in (*a*) backscattering and (*b*) the 90° detectors. Black arrows indicate scattering from vanadium in the sample environment.

electronic reprint

Table 1
Powder data, atomic coordinates, displacement parameters, and selected bond lengths and angles for α-$MgSO_4$ at 4.2 K.

		Fitted		Minus background	
Histogram	N_{obs}	wRp	Rp	wRp	Rp
Backscattering	4046	0.0439	0.0360	0.0434	0.0350
90° banks	1583	0.0310	0.0240	0.0261	0.0224
Powder totals	5629	0.0356	0.0288	0.0321	0.0278
χ^2 = 3.892					

Space group	a (Å)	b (Å)	c (Å)	V (Å^3)	ρ (kg m^{-3})
Cmcm, Z = 4	5.168629 (33)	7.867806 (54)	6.466744 (54)	262.975 (2)	3040.16 (2)

Atom label	x	y	z	$U_{iso} \times 100$ (Å^2)
Mg	0	0	0	0.85 (3)
S	0	0.3511 (2)	0.25	0.79 (5)
O1	0	0.24966 (8)	0.06264 (9)	0.82 (2)
O2	0.23394 (14)	0.46246 (7)	0.25	0.83 (2)

Interatomic distances (Å) and angles (°)			
S—O1	1.4507 (11)	O1—S—O1	113.28 (12)
S—O2	1.4934 (11)	O1—S—O2	108.83 (2)
Mg—O1	2.0056 (6)	O2—S—O2	108.12 (12)
Mg—O2	2.1429 (5)	Mg—O1—S	135.01 (6)
Mg—Mg	3.23337(3)	Mg—O2—S	126.91 (2)
Mg—S	3.2004 (14)	O2—Mg—O2	79.84 (3)
O2—O2	2.7503 (10)		

Table 2
Powder data, atomic coordinates, displacement parameters, and selected bond lengths and angles for β-$MgSO_4$ at 4.2 K.

		Fitted		Minus background	
Histogram	N_{obs}	wRp	Rp	wRp	Rp
Backscattering	4256	0.0544	0.0462	0.0549	0.0468
90° banks	1422	0.0472	0.0364	0.0476	0.0378
Powder totals	5678	0.0498	0.0416	0.0497	0.0425
χ^2 = 6.232					

Space group	a (Å)	b (Å)	c (Å)	V (Å^3)	ρ (kg m^{-3})
Pbnm, Z = 4	4.73431 (8)	8.58170 (12)	6.67266 (11)	271.100 (5)	2949.04 (5)

Atom label	x	y	z	$U_{iso} \times 100$ (Å^2)
Mg	0	0	0	0.59 (4)
S	0.4817 (7)	0.1804 (3)	0.25	0.89 (7)
O1	0.77592 (30)	0.12657 (25)	0.25	0.80 (4)
O2	0.46283 (28)	0.35178 (14)	0.25	0.68 (4)
O3	0.33849 (22)	0.12604 (12)	0.06902 (13)	0.82 (3)

Interatomic distances (Å) and angles (°)			
S—O1	1.468 (4)	O1—S—O2	111.81 (24)
S—O2	1.4736 (25)	O1—S—O3	109.87 (13)
S—O3	1.4612 (18)	O2—S—O3	106.89 (13)
Mg—O1	2.2557 (13)	O3—S—O3	111.47 (22)
Mg—O2	2.1052 (8)	Mg—O1—S	126.72 (6)
Mg—O3	1.9875 (11)	Mg—O2—S	126.73 (4)
Mg—Mg	3.33633 (6)	Mg—O3—S	137.66 (12)
Mg—S	3.2115 (19)	O1—Mg—O2	75.18 (5)
Mg—S	3.2216 (27)		
O1—O2	2.6628 (24)		

refined the diffractometer constants DIFA and DIFC, since these quantities are less well determined from the NBS silicon standard than for the backscattering detector bank. Small segments of data were excluded at the top end of the backscattering histograms, and from both ends of the 90° histograms, owing to normalization errors at the edges of the time-of-flight window. In the β-$MgSO_4$ 90° data, two spurious unidentified peaks near 2.5 and 2.6 Å were excluded; a small, rather broad, feature near 2.4 Å in the α-$MgSO_4$ 90° data was ignored, as were other small peaks due to vanadium at ~2.1 Å (these appear as a broad hump or doublet from the front and back windows of the cryostat and inner vacuum vessel), but these are indicated by arrows in Fig. 3. Powder statistics and structural parameters for these refinements are given at the top of Tables 1 and 2.

The structure refinements at 4.2 K were then used as the basis for refining the data collected during the warming runs; at each datum, atomic positions, isotropic displacement parameters, scale factors, background and profile coefficients were refined in turn. At 300 K, the data were refined with anisotropic thermal motion for the Mg and O atoms. In β-$MgSO_4$, even with soft restraints on the S—O distance, anisotropic refinement of atom O1 resulted in an unphysical value of U_{11} (*i.e.* it was negative). However, inspection of the oxygen displacement ellipsoids shows that these atoms are vibrating orthogonally (see §3.3), so it was considered appropriate to set U_{11}(O1) = U_{22}(O2) = U_{33}(O3) and then constrain the shifts to be equal during refinement; this ultimately resulted in a stable and physical solution, although the quality of the fit for β-$MgSO_4$ is clearly not quite as good as it is for α-$MgSO_4$ (compare Figs. 3 and 4). Powder statistics for the 300 K refinements are given at the top of Tables 3 and 4. All of the raw diffraction data, *GSAS* Expgui files and *GSAS* Listview files may be found in the supplementary electronic materials.[1] Results pertaining to peak profile and background coefficients, as well as powder statistics, for each datum are also contained in this deposit.

3. Results

3.1. Structures at 4.2 and 300 K

The structural parameters reported here represent a considerable improvement in precision over the existing data; the refined atomic positions and displacement parameters for both phases at 4.2 and 300 K are given in Tables 1–4. Note that the precision of the location and thermal motion of the S atoms is poorer than that for the other atoms because of the very much smaller neutron scattering cross section of sulfur. Also given in Tables 1–4 are selected interatomic bond lengths

[1] Supplementary data for this paper are available from the IUCr electronic archives (Reference: DB5013). Services for accessing these data are described at the back of the journal.

electronic reprint

Table 3
Powder data, atomic coordinates, displacement parameters, and selected bond lengths and angles for α-$MgSO_4$ at 300 K.

		Fitted		Minus background	
Histogram	N_{obs}	wRp	Rp	wRp	Rp
Backscattering	4070	0.0381	0.0314	0.0335	0.0283
90° banks	1373	0.0284	0.0223	0.0230	0.0196
Powder totals	5443	0.0320	0.0265	0.0264	0.0233
$\chi^2 = 3.131$					

Space group	a (Å)	b (Å)	c (Å)	V (Å^3)	ρ (kg m^{-3})
Cmcm, $Z = 4$	5.174713 (29)	7.875632 (48)	6.495166 (46)	264.705 (2)	3020.29 (2)

Atom label	x	y	z	$U \times 100$ (Å^2)	
Mg	0	0	0	$U_{11} = 1.44$ (7)	$U_{12} = 0$
				$U_{22} = 1.35$(7)	$U_{13} = 0$
				$U_{33} = 0.97$(7)	$U_{23} = -0.02$(4)
S	0	0.3508 (2)	0.25	$U_{iso} = 1.05$ (4)	
O1	0	0.24939 (8)	0.06357 (9)	$U_{11} = 1.25$ (4)	$U_{12} = 0$
				$U_{22} = 1.29$ (4)	$U_{13} = 0$
				$U_{33} = 1.29$ (3)	$U_{23} = -0.37$ (3)
O2	0.23321 (14)	0.46184 (7)	0.25	$U_{11} = 0.93$ (4)	$U_{12} = -0.34$ (3)
				$U_{22} = 1.48$(4)	$U_{13} = 0$
				$U_{33} = 1.16$(4)	$U_{23} = 0$

Interatomic distances (Å) and angles (°)			
S—O1	1.4505 (10)	O1—S—O1	113.20 (12)
S—O2	1.4904 (10)	O1—S—O2	108.85 (2)
Mg—O1	2.0071 (6)	O2—S—O2	108.13 (12)
Mg—O2	2.1524 (5)	Mg—O1—S	135.27 (6)
Mg—Mg	3.24758 (2)	Mg—O2—S	126.96 (2)
Mg—S	3.2045 (14)	O2—Mg—O2	79.79(3)
O2—O2	2.7611 (10)		

and angles. With the level of precision attainable with our data it is possible to elucidate the differences between the two polytypes which result in their different densities. Although differing in their packing, as described in §1, the lateral distance between MgO_6 chains is only marginally different (measured from the central Mg atom, 4.707 Å in α-$MgSO_4$ and 4.734 Å in β-$MgSO_4$ at 300 K), as is the vertical separation between adjacent layers of MgO_6 octahedra (4.330 Å in α-$MgSO_4$ and 4.291 Å in β-$MgSO_4$). Indeed, the main difference between the two polytypes is in the separation of Mg atoms along the MgO_6 ribbons. In α-$MgSO_4$, the distance from the Mg atom to the shared edge (or hinge) of the octahedra is 1.6513 Å (and the hinge itself is 2.7611 Å wide), which, given the Mg···Mg distance of 3.24758 Å, requires that each MgO_6 polyhedron be tilted by 10.47° (Fig. 5) perpendicular to the plane of cross-linked sheets. In β-$MgSO_4$, the equivalent Mg···Mg distance along the ribbons is 3.35467 Å. Given that the Mg—O distances are actually marginally smaller than in the α phase, the only way this can be accommodated is by shrinking the width of the hinge (down to 2.6716 Å or −3.2%) and increasing the Mg–hinge distance (up to 1.7424 Å or +5.5%), resulting in an increase in the tilt of the MgO_6 polyhedron from 10.47 to 15.71° (+50.0%).

Table 4
Powder data, atomic coordinates, displacement parameters, and selected bond lengths and angles for β-$MgSO_4$ at 300 K.

		Fitted		Minus background	
Histogram	N_{obs}	wRp	Rp	wRp	Rp
Backscattering	4297	0.0541	0.0463	0.0515	0.0453
90° banks	1404	0.0380	0.0293	0.0359	0.0304
Powder totals	5701	0.0440	0.0375	0.0406	0.0376
$\chi^2 = 4.157$					

Space group	a (Å)	b (Å)	c (Å)	V (Å^3)	ρ (kg m^{-3})
Pbnm, $Z = 4$	4.74598 (7)	8.58310 (10)	6.70933 (9)	273.306 (4)	2925.42 (4)

Atom label	x	y	z	$U \times 100$ (Å^2)	
Mg	0	0	0	$U_{11} = 1.86$ (13)	$U_{12} = -0.35$ (10)
				$U_{22} = 1.10$ (8)	$U_{13} = 0.28$ (8)
				$U_{33} = 0.98$ (11)	$U_{23} = 0.73$ (10)
S	0.4780 (4)	0.1812 (2)	0.25	$U_{iso} = 1.29$ (7)	
O1	0.77090 (29)	0.12651 (26)	0.25	$U_{11} = 0.34$ (5)	$U_{12} = -0.29$ (8)
				$U_{22} = 0.73$ (10)	$U_{13} = 0$
				$U_{33} = 2.92$ (10)	$U_{23} = 0$
O2	0.46410 (40)	0.35189 (14)	0.25	$U_{11} = 3.00$ (13)	$U_{12} = 0.55$ (10)
				$U_{22} = 0.34$ (5)	$U_{13} = 0$
				$U_{33} = 0.89$ (9)	$U_{23} = 0$
O3	0.33748 (23)	0.12661 (14)	0.06959 (14)	$U_{11} = 1.43$ (7)	$U_{12} = -0.27$ (7)
				$U_{22} = 2.68$ (7)	$U_{13} = -0.22$ (5)
				$U_{33} = 0.34$ (5)	$U_{23} = 0.07$ (8)

Interatomic distances (Å) and angles (°)			
S—O1	1.4674 (17)	O1—S—O2	111.22 (19)
S—O2	1.4666 (16)	O1—S—O3	109.28 (9)
S—O3	1.4592 (11)	O2—S—O3	107.47 (10)
Mg—O1	2.2748 (13)	O3—S—O3	112.10 (17)
Mg—O2	2.1115 (8)	Mg—O1—S	127.27 (5)
Mg—O3	1.9910 (10)	Mg—O2—S	126.72 (3)
Mg—Mg	3.35467 (5)	Mg—O3—S	137.50 (11)
Mg—S	3.2214 (18)	O1—Mg—O2	74.95 (5)
Mg—S	3.2113 (14)		
O1—O2	2.6716 (25)		

3.2. Thermal expansion

Fig. 6 shows the refined unit-cell dimensions for α-$MgSO_4$ and β-$MgSO_4$ as a function of temperature; note that in all cases, with the obvious exception of the β-phase b axis, the standard errors are smaller than the symbols employed. It is clear that the thermal expansion of the three crystallographic axes of α-$MgSO_4$ is positive and normally behaved at all temperatures. However, for β-$MgSO_4$, whilst the expansion of the a and c axes, and the volume thermal expansion coefficient, are positive at all temperatures and normally behaved, the thermal expansion of the b axis is both very small and

electronic reprint

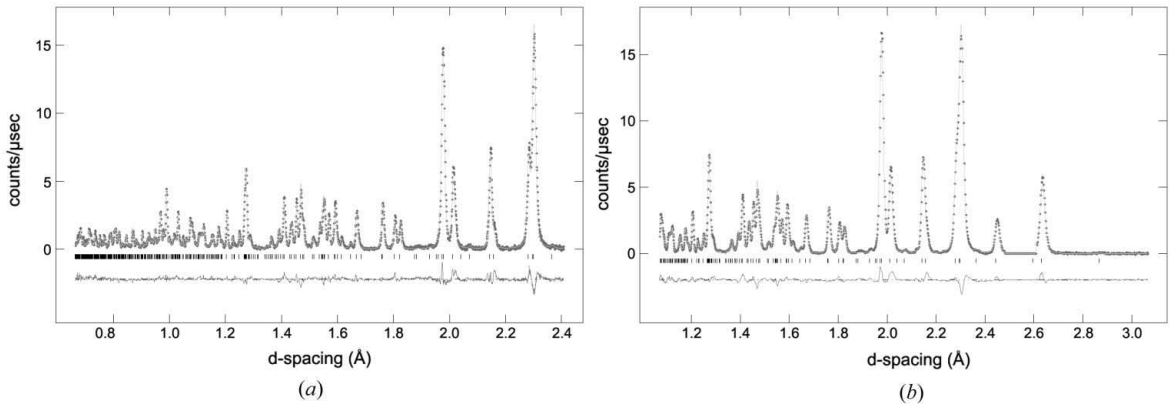

Figure 4
Powder diffraction data (points), Rietveld refinement (solid line fitted through the data), difference profile and tic marks (bottom) for β-$MgSO_4$ at 4.2 K in (*a*) backscattering and (*b*) the 90° detectors.

negative below ~125 K. We have observed similar behaviour in the *a* axis of $MgSO_4{\cdot}7D_2O$ (Fortes *et al.*, 2006).

In this subsection we analyse the thermal expansion in terms of the internal energy of the crystal. The volume thermal expansion of both α- and β-$MgSO_4$ is parameterized in terms of a simple Debye model of the internal energy. The axial expansivities are also parameterized in terms of a Debye model; in the sole instance of the *b* axis of β-$MgSO_4$, which exhibits negative thermal expansion, we adopt a mixed Debye–Einstein model parameterized in terms of two characteristic vibrational temperatures.

Our description of the thermal expansion begins with Grüneisen's relation between the thermoelastic parameters,

$$\gamma = \alpha_V V K_T / C_V, \qquad (1)$$

where γ is the Grüneisen ratio, α_V is the volume thermal expansion coefficient, K_T is the isothermal bulk modulus, C_V is the isochoric specific heat capacity and V is the unit-cell volume. If γ and K_T are assumed to be independent of temperature, integration of equation (1) with respect to T leads to the following expression for the thermal expansion in terms of the internal energy of the crystal,

$$V(T) = V_0 + \gamma U(T)/K_T, \qquad (2)$$

where V_0 is the volume at 0 K. The internal energy, $U(T)$, may be obtained *via* a Debye approximation for the heat capacity (*e.g.* Wallace, 1998),

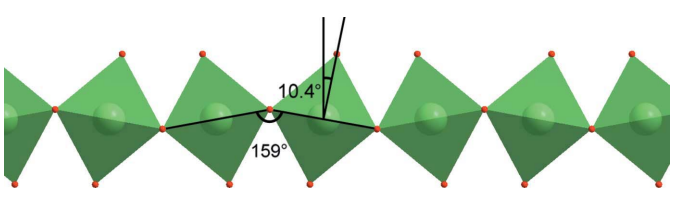

Figure 5
Schematic of the tilting between adjacent MgO_6 octahedra in α-$MgSO_4$ along the length of the edge-sharing chains; O1 is the apical O atom and O2 forms the shared edge. In β-$MgSO_4$, the shared edge is formed by O1···O2 and O3 is the apical O atom.

$$U(T) = 9Nk_BT(T/\theta_D)^3 \int_0^{\theta_D/T} x^3/[\exp(x)-1]\,dx, \qquad (3)$$

where N is the number of atoms in the unit cell, k_B is Boltzmann's constant, θ_D is the Debye temperature and $x = \hbar\omega/k_BT$. Note that the vibrational zero-point energy of $9Nk_B\theta_D/8$ is included in equation (2) *via* the term V_0.

In previous studies, we have found that this expression, or similar expressions taken to higher order, are capable of modelling accurately the thermal expansion of simple inorganic solids (Vočadlo *et al.*, 2002; Wood *et al.*, 2002, 2004) over a wide temperature range, thereby providing a method of estimating both their Debye temperatures and their elastic parameters. However, in the case of molecular solids (Fortes *et al.*, 2003, 2005, 2006) the presence of both inter- and intramolecular vibrations means that a more realistic calculation of the internal energy, for example using a double Debye model (*i.e.* with two characteristic Debye temperatures) fitted to experimental heat capacity data, may be required if physically sensible elastic parameters are to be extracted from $V(T)$ data.

The specific heat capacity of anhydrous $MgSO_4$ was measured by Moore & Kelley (1942) from 53 to 295 K. Their specimen was formed by dehydration of $MgSO_4{\cdot}7H_2O$ and is thus quite likely to have been β-$MgSO_4$; however, we cannot be absolutely certain which phase Moore and Kelly's specimen was. We have therefore fitted Debye models to the heat capacity data of Moore & Kelley (1942) *for purely comparative purposes* rather than to provide Debye temperatures for fitting $V(T)$ as we have done previously. The isochoric data of Moore & Kelley (1942) were converted to isobaric values using $C_P = C_V(1 + \alpha_V\gamma T)$, with α_V taken to be that measured by us for β-$MgSO_4$ and $\gamma = 1$. Single and double Debye models were fitted (Fig. 7), the latter providing by far the better fit to the data. For the single Debye model, we obtained θ_D = 520 (130) K, and for the double Debye model we found θ_{D1} = 365 (3) K and θ_{D2} = 1094 (6) K (corresponding to vibrational wavenumbers of ~250 cm^{-1} and ~760 cm^{-1}, respectively). The value of θ_{D1} is in close agreement with that obtained from fitting the unit-cell volume of β-$MgSO_4$ (see below).

electronic reprint

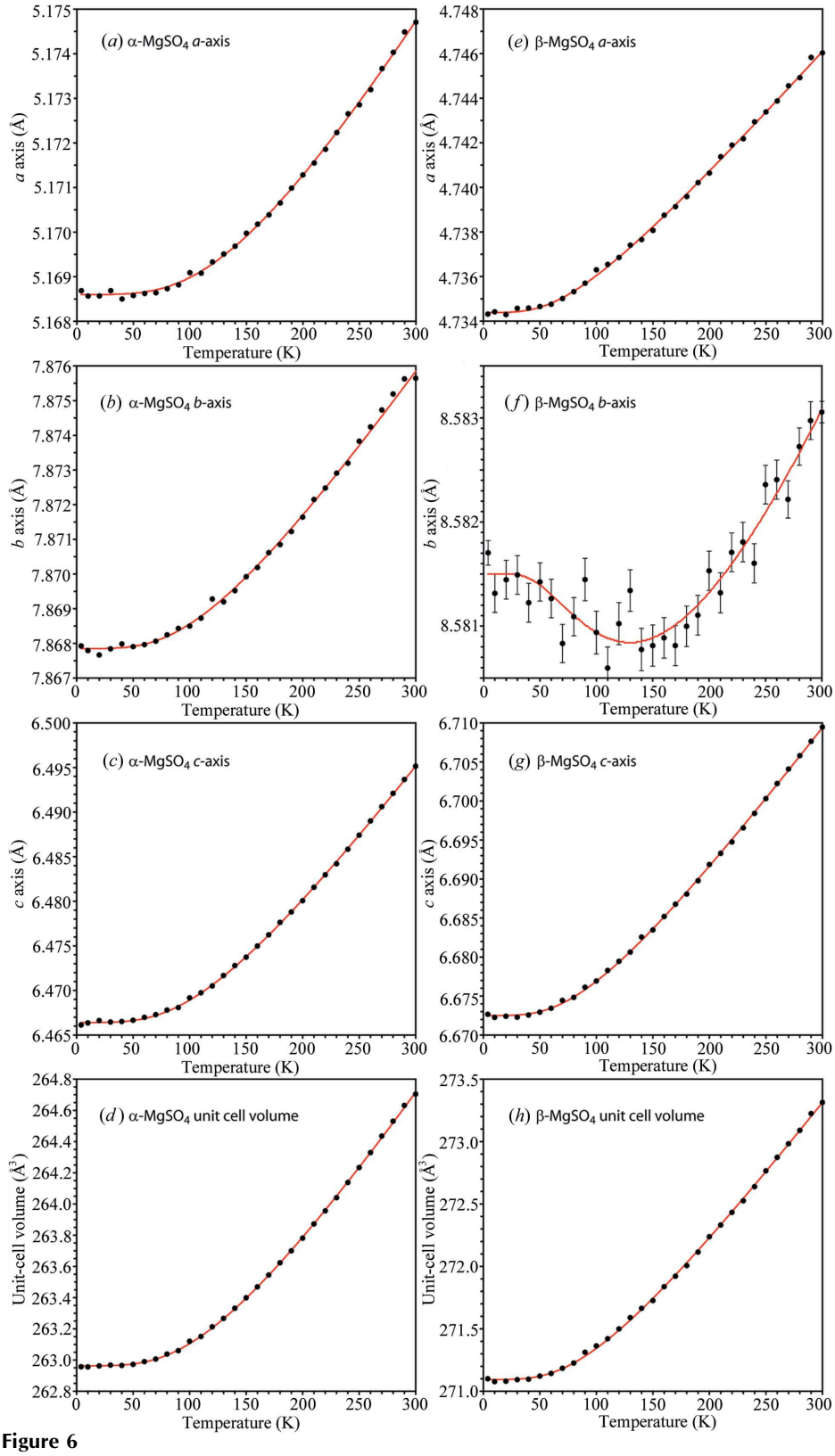

Figure 6
Temperature dependence of the unit-cell edge lengths and volume for α-$MgSO_4$ (*a*–*d*) and β-$MgSO_4$ (*e*–*h*). Solid lines are weighted least-squares fits of the Debye model described in the text. For the *b* axis of β-$MgSO_4$ (*f*) the solid line is a combined Debye + Einstein model. For all plots except (*f*) (where the errors bars are given), standard errors are of the same size as, or smaller than, the symbols used. (*f*) has an expanded vertical scale as a result of the very small variation in the length of the *b* axis of β-$MgSO_4$ with temperature. The data used in the preparation of these plots may be found in supplementary electronic files deposited with the IUCr.

The results of weighted nonlinear least-squares fits of equation (2) to the unit-cell volumes of α- and β-$MgSO_4$ are given in Table 5 and shown in Figs. 6(*d*) and 6(*h*). It can be seen that a very good fit to the $V(T)$ data has been obtained for both phases. The alternative approach of using an Einstein model (see below) for $U(T)$ was also tried as this has been used successfully to model the thermal expansion of inorganic substances, such as crocoite, $PbCrO_4$ (Knight, 1996), and perdeuterated gypsum, $CaSO_4{\cdot}2D_2O$ (Knight *et al.*, 1999). However, although this method has the advantage of greater mathematical simplicity, it was found to give a fit to the data in the region of curvature (*i.e.* between about 50 and 150 K) that was noticeably less good.

Despite their structural similarities, there is a significant difference in the estimated Debye temperatures of the two phases, with θ_D for α-$MgSO_4$ over 100 K higher than for β-$MgSO_4$. The values of K_T/γ, ~85 GPa for both phases (Table 5), are physically reasonable, as our unpublished density functional theory calculations indicate that K_T is ~64 GPa for the α phase.

Strictly, equation (2) applies to the volume of the crystal, but in the form

$$x(T) = x_0 + x_1 U(T) \qquad (4)$$

it was found also to give a good fit to the individual lattice parameters (see below). Clearly, however, equation (4) is not capable of modelling the behaviour of the *b* axis of β-$MgSO_4$. It seemed likely that the contraction of this axis at low temperatures was due to one or more low-frequency rigid-body rotational modes of the SO_4 tetrahedra or MgO_6 octahedra. An additional term was, therefore, introduced into equation (4), which becomes

$$b(T) = b_0 + b_1 U_1(T) + b_2 U_2(T). \qquad (5)$$

electronic reprint

Table 5
Parameters resulting from the fitting of the Debye model [equations (2) and (3)] to the measured unit-cell volumes.

	V_0 (Å^3)	K/γ (GPa)	θ_D (K)
α-$MgSO_4$	262.963 (2)	88.5 (8)	483 (5)
β-$MgSO_4$	271.094 (4)	82.2 (7)	371 (6)

Table 6
Parameters resulting from the fitting of the Debye model [equations (3) and (4)] to the measured unit-cell parameters, and of a combined Debye + Einstein model to the b axis of β-$MgSO_4$ [equations (3), (5) and (6)].

	x_0 (Å)	x_1	x_2	θ_D (K)	θ_E (K)
α-$MgSO_4$					
a	5.16860 (2)	4.5 (1) × 10^{-14}	–	576 (13)	–
b	7.86785 (4)	4.9 (1) × 10^{-14}	–	452 (18)	–
c	6.46641 (5)	17.8 (2) × 10^{-14}	–	457 (6)	–
β-$MgSO_4$					
a	4.73439 (4)	5.80 (7) × 10^{-14}	–	297 (9)	–
b	8.58150 (8)	6.0 (3) × 10^{-14}	−3.0 × 10^{-14}†	598 (77)	185 (33)
c	6.67250 (7)	19.8 (2) × 10^{-14}	–	353 (5)	–

Since the mode is assumed to cause contraction of the structure parallel to the b axis, the Grüneisen ratio for the final term in equation (5) is taken to be negative, *i.e.* $b_2 < 0$. As before, $U_1(T)$ was calculated using the Debye approximation, but an Einstein model (*e.g.* Wallace, 1998), corresponding to a single mode of fixed frequency with characteristic temperature θ_E, was used to obtain $U_2(T)$, where

$$U_2(T) = 3Nk_B\theta_E/[\exp(\theta_E/T) - 1]. \qquad (6)$$

The results of fitting equations (4) and (5) to the lattice parameters are shown in Figs. 6(*a*)–6(*c*) and 6(*e*)–6(*g*), with the values of the fitted parameters given in Table 6. Free refinement of all five variables in equation (5) was found not to be possible and so the parameter b_2 was adjusted manually until the best fit to the data was obtained. It can be seen from Fig. 6 that these models gave very good representations of the behaviour of all of the cell parameters. It is interesting to note that the mean values of the characteristic temperatures obtained from the cell edges, 495 (21) K for α-$MgSO_4$ and 358 (21) K for β-$MgSO_4$, agree very well with those obtained from fitting the cell volumes, 483 (5) and 371 (6) K, respectively.

The fitted parameters from Tables 5 and 6 were then used to calculate the magnitude of the volumetric thermal expansion coefficient as a function of temperature, $\alpha_V(T)$. The anisotropic thermal expansion of an orthorhombic crystal is given by a second-rank tensor with all off-diagonal terms zero; the non-zero diagonal terms, $\alpha_{11} = a^{-1}(\partial a/\partial T)$, $\alpha_{22} = b^{-1}(\partial b/\partial T)$ and $\alpha_{33} = c^{-1}(\partial c/\partial T)$, are the magnitudes of the principal axes,

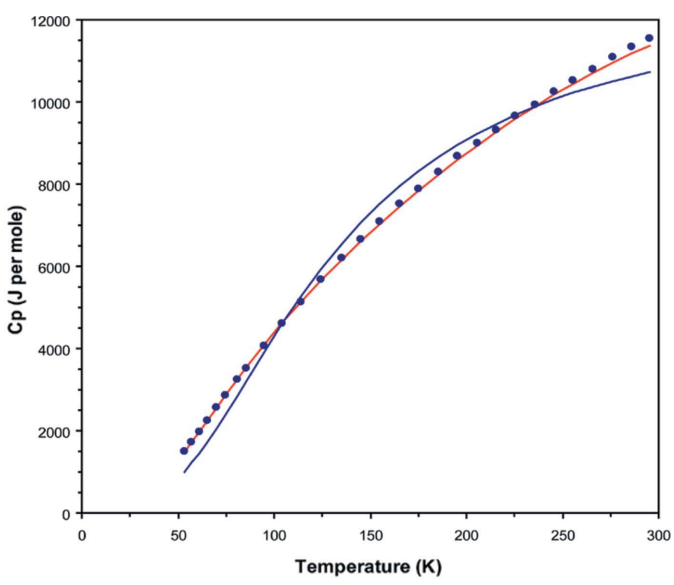

Figure 7
Single Debye (blue line) and double Debye (red line) fits to the specific heat capacity data of Moore & Kelley (1942).

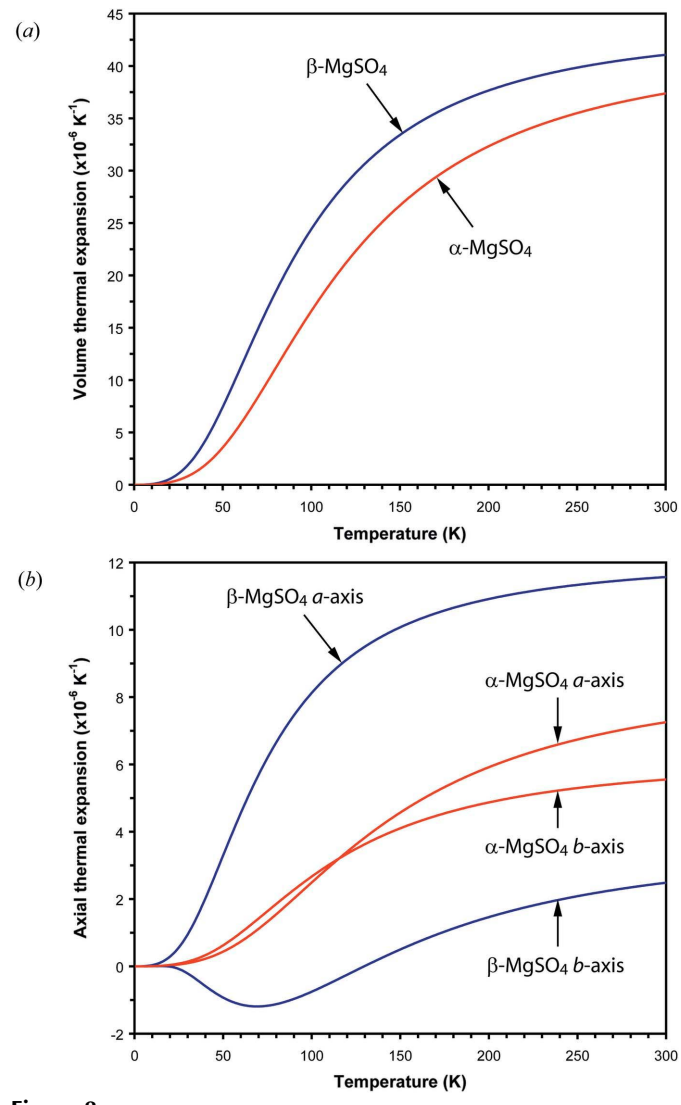

Figure 8
(*a*) The calculated values of the volume thermal expansion coefficients, α_V, for both α-$MgSO_4$ (red) and β-$MgSO_4$ (blue). (*b*) The calculated values of the axial thermal expansion coefficients, α_{11} and α_{22}, for α-$MgSO_4$ (red) and β-$MgSO_4$ (blue).

electronic reprint

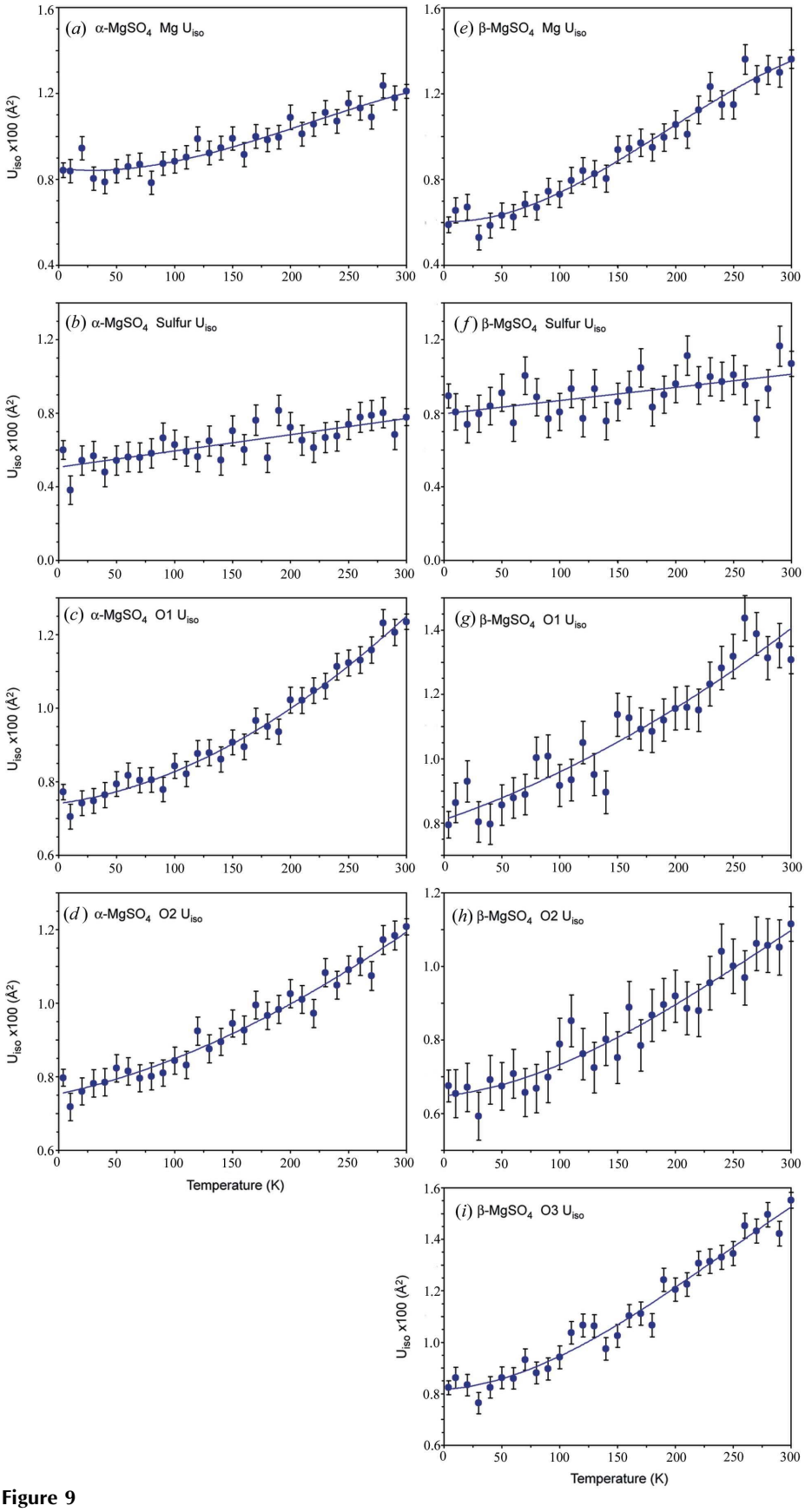

Figure 9
Temperature dependence of the isotropic displacement parameters in α-$MgSO_4$, (*a*) Mg, (*b*) S, (*c*) O1 and (*d*) O2, and in β-$MgSO_4$, (*e*) Mg, (*f*) S, (*g*) O1, (*h*) O2 and (*i*) O3. The data used in the preparation of these plots may be found in supplementary electronic files deposited with the IUCr.

α_1, α_2 and α_3, of the thermal expansion tensor (the directions being fixed by the crystal symmetry). Fig. 8(*a*) shows $\alpha_V(T)$ for α-$MgSO_4$ and β-$MgSO_4$. For both phases, α_{33} is much larger than α_{11} or α_{22}, and the temperature dependences of α_{33} are similar to those of α_V. However, Fig. 8(*b*) shows that there are some interesting differences in $\alpha_{11}(T)$ and $\alpha_{22}(T)$. At 300 K, the axial and volume expansivities for α-$MgSO_4$ are α_{11} = 7.3 (1) $\times 10^{-6}$ K^{-1}, α_{22} = 5.6 (2) $\times 10^{-6}$ K^{-1}, α_{33} = 24.3 (2) $\times 10^{-6}$ K^{-1} and α_V = 37.4 (3) $\times 10^{-6}$ K^{-1}. At 300 K, the expansivities for β-$MgSO_4$ are α_{11} = 11.6 (3) $\times 10^{-6}$ K^{-1}, α_{22} = 2.5 (2) $\times 10^{-6}$ K^{-1}, α_{33} = 27.3 (3) $\times 10^{-6}$ K^{-1} and α_V = 41.1 (5) $\times 10^{-6}$ K^{-1} (the values quoted are those obtained using the parameters given in Tables 5 and 6, with the estimated standard errors derived from linear fits to the data above 200 K).

In β-$MgSO_4$, the large expansivity of the *c* axis is associated with the expansion of the MgO_6 chains along their length, and the very small expansivity of the *b* axis is a direct measure of the expansion perpendicular to the SO_4 sheets. The *a*-axis expansion reflects the increasing separation of adjacent MgO_6 ribbons. In α-$MgSO_4$, the structural expansion is similar but is manifested slightly differently as the pseudo-close-packed layering is parallel to $(\bar{1}10)$ rather than (010) in the β phase. In both phases, the expansion along the octahedral ribbons is due to expansion of the octahedra themselves; the hinge angle in α-$MgSO_4$ only increases from 10.33 to 10.47° between 4 and 300 K, and in β-$MgSO_4$ from 15.30 to 15.71°.

3.3. Thermal motion

The isotropic displacement parameters for each atom were refined at each temperature datum; results for both phases are shown in Fig. 9. Isotropic displacement parameters at 4.2 K and anisotropic parameters

electronic reprint

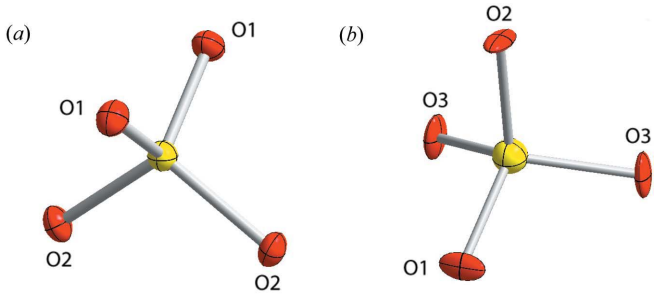

Figure 10
Displacement ellipsoid plots (50% probability) for the sulfate groups in (*a*) α-$MgSO_4$ and (*b*) β-$MgSO_4$ at 300 K; atom labels are those employed in the text and in Tables 1–4.

at 300 K also appear in Tables 1–4 (displacement ellipsoids for the sulfate groups in both phases are shown in Fig. 10).

Of particular note is the rate at which the thermal motion increases as a function of temperature. In α-$MgSO_4$, the thermal motion of the edge-sharing O atom (O2) is increasing at a rate of 2.4 (4) $\times$ 10^{-5} Å^2 K^{-1} at 300 K (calculated by differentiation of the fitted polynomial) and that of the apical O atom (O1) is increasing at a rate of 2.9 (3) $\times$ 10^{-5} Å^2 K^{-1} at 300 K. In β-$MgSO_4$, the thermal motions of the edge-sharing O atoms (O1 and O2) are increasing at a rate of 2.3 (9) $\times$ 10^{-5} Å^2 K^{-1} and 2.6 (6) $\times$ 10^{-5} Å^2 K^{-1}, respectively, at 300 K, whereas that of the apical O atom (O3) is significantly larger, increasing at a rate of 3.9 (7) $\times$ 10^{-5} Å^2 K^{-1}. Similarly, there is a large difference in the rate of increase of the thermal motion of the Mg atom between the two structures; at 300 K the rate is 2.3 (6) $\times$ 10^{-5} Å^2 K^{-1} in α-$MgSO_4$ and 3.9 (7) $\times$ 10^{-5} Å^2 K^{-1} in β-$MgSO_4$. The rate of increase in the thermal motion of the S atoms in the two structures is virtually identical, being 0.8 (1) $\times$ 10^{-5} Å^2 K^{-1} in α-$MgSO_4$ and 0.7 (2) $\times$ 10^{-5} Å^2 K^{-1} in β-$MgSO_4$.

4. Summary

We have carried out detailed neutron powder diffraction measurements on two polymorphs of anhydrous magnesium sulfate. Our structure refinements at 4.2 and 300 K are of higher precision than existing reported structures. We have also measured the axial and volumetric thermal expansion coefficients over the range 4.2 K $< T <$ 300 K, as well as determining structural and thermal parameters as a function of temperature, though with lower precision than at the end points. These results provide the basis for the fitting of interatomic potentials, which will be expanded upon in a subsequent paper.

The authors are grateful to the ISIS facility for beam time to carry out this experiment and to the ISIS support staff for technical assistance. ADF, LV, and HEAB are, respectively, supported by STFC (grant No. PPA/P/S/2003/00247), the Royal Society, and a postgraduate studentship from NERC.

References

Coing-Boyat, J. (1962). *C. R. Acad. Sci. Paris*, **255**, 1962–1964.
Daimon, K. & Kato, E. (1984). *Yogyo Kyokai Shi*, **92**, 153–155.
Fortes, A. D., Wood, I. G., Alfredsson, M., Vočadlo, L. & Knight, K. S. (2005). *J. Appl. Cryst.* **38**, 612–618.
Fortes A. D., Wood, I. G., Alfredsson, M., Vočadlo, L. & Knight, K. S. (2006). *Eur. J. Mineral.* **18**, 449–462.
Fortes, A. D., Wood, I. G., Brodholt, J. P., Knight, K. S., Alfredsson, M., McGrady, G. S. & Vočadlo, L. (2003). *J. Chem. Phys.* **119**, 10806–10813.
Fortes, A. D., Wood, I. G., Vočadlo, L. & Alfredsson, M. (2004). ISIS Experimental Report RB15133, Rutherford Appleton Laboratory, Oxfordshire, UK.
Ibberson, R. M., David, W. I. F. & Knight, K. S. (1992). *The High Resolution Neutron Powder Diffractometer (HRPD) at ISIS – A User Guide*. RAL-92-031. Rutherford Appleton Laboratory, Oxfordshire, UK.
Kargel, J. S. (1991). *Icarus*, **94**, 368–390.
Kargel, J. S., Kirk, R. L., Fegley, B. & Treiman, A. H. (1994). *Icarus*, **112**, 219–252.
Knight, K. S. (1996). *Mineral. Mag.* **60**, 963–973.
Knight, K. S., Stretton, I. C. & Schofield, P. F. (1999). *Phys. Chem. Miner.* **26**, 477–483.
Larson, A. C. & von Dreele, R. B. (1988). *General Structure Analysis System* (*GSAS*). Report LAUR B6-748. Los Alamos National Laboratory, New Mexico, USA.
Livshits, L. D., Genshaft, Yu. S. & Ryabin, Yu. N. (1963). *Russ. J. Inorg. Chem.* **8**, 676–678.
Moore, G. E. & Kelley, K. K. (1942). *J. Am. Chem. Soc.* **64**, 2949–2951.
Rentzeperis, P. J. & Soldatos, C. T. (1958). *Acta Cryst.* **11**, 686–688.
Rowe, J. J., Morey, G. W. & Silber, C. C. (1967). *J. Inorg. Nucl. Chem.* **29**, 925–942.
Vočadlo, L., Knight, K. S., Price, G. D. & Wood, I. G. (2002). *Phys. Chem. Miner.* **29**, 132–139.
Wallace, D. C. (1998). *Thermodynamics of Crystals*. New York: Dover.
Wang, Y. C., Akaishi, M. & Yamaoka, S. (1999). *Diamond Relat. Mater.* **8**, 73–77.
Wood, I. G., Knight, K. S., Price, G. D. & Stuart, J. A. (2002). *J. Appl. Cryst.* **35**, 291–295.
Wood, I. G., Vočadlo, L., Knight, K. S., Dobson, D. P., Marshall, W. G., Price, G. D. & Brodholt, J. (2004). *J. Appl. Cryst.* **37**, 82–90.
Yamaguchi, A. & Kato, E. (1972). *Yogyo Kyokai Shi*, **80**, 337–339.

electronic reprint